RSC Advances

PAPER

View Article Online
View Journal | View Issue

Cite this: *RSC Adv.*, 2017, **7**, 15222

Luminescence properties and energy transfer in Tb^{3+} and Eu^{3+} co-doped $Ba_2P_2O_7$ phosphors

Baoxing Wang,* Qiang Ren, Ou Hai and Xiulan Wu

Received 13th December 2016
Accepted 27th February 2017

DOI: 10.1039/c6ra28122b

rsc.li/rsc-advances

The $Ba_2P_2O_7$:Tb^{3+}, Eu^{3+} phosphors were synthesized by a high temperature solid-state reaction method in air atmosphere and their crystal structures, lifetime, luminescence properties, and energy transfer mechanism were investigated in detail. A series of characteristic emissions of $Ba_2P_2O_7$:Tb^{3+}, Eu^{3+} phosphors were observed in the emission spectra at around 545 nm, 593 nm, and 613 nm when excited at 378 nm. The energy-transfer mechanism from Tb^{3+} to Eu^{3+} in $Ba_2P_2O_7$ is determined by a dipole–dipole interaction. The emission intensity of $Ba_{2-x}P_2O_7$:xEu^{3+} was enhanced by doping charge compensation Li^+, Na^+ and K^+. The CIE coordinates of the phosphors can be tuned from blue-green through white, to yellow and finally to orange-red with changing the Eu^{3+}/Tb^{3+} ratio. The average decay time of Eu^{3+} increases from 2.10 to 5.81 ms with the concentration of Tb^{3+} increasing from 2% to 8%, and reaches the maximum at 0.08, and is shortened when the concentration of Tb^{3+} goes beyond 8%.

1. Introduction

Nowadays, as the next-generation lighting and display systems, the white light-emitting diodes (WLEDs) are attracting much attention due to their environmental friendliness, reliability, and low power consumption.[1–5,28,29] In general, the manufacture of white light phosphors follows one of two routes. One approach is to mix monochromatic (red/green/blue) phosphors in the best proportion, the other approach is to excite yellow phosphors using blue or ultraviolet (UV) emitting chips.[6] However, for phosphor mixtures, the strong re-absorption and nonuniformity of luminescence problems exist, this result gives rise to the loss of luminescence efficiency, properties, and multicolor emitting points. Compared with phosphor mixtures, a single phase phosphor has more advantages and overcomes these problems. So, the single phase phosphor is a very promising material.[7–9,30,31]

Recently, more and more scholars focus on pyrophosphate phosphor materials which have the advantage of environmental friendliness, chemical stability, low power consumption, and high efficiency, *etc.*[10] In the rare earth family, due to the existence of $^5D_3$–$^7F_5$, and $^5D_4$–$^7F_5$ transition, the Tb^{3+} ion doped phosphors which can emit blue and green light has been prepared in previous research. Meanwhile, Eu^{3+} ion is a red emitting activator due to its $^5D_0$–$^7F_2$ transition.[6] Accordingly, the Tb^{3+} and Eu^{3+} co-doped phosphors can generate simultaneous the red/green/blue emissions. At present, by means of the energy-transfer from a sensitizer to an activator, the multicolor emitting phosphor can be usually designed under ultraviolet excitation, so by co-doping of Eu^{3+} and Tb^{3+} ions, the color emission may be tuned base on the energy transfer from Tb^{3+} to Eu^{3+}. In some literatures, the Tb^{3+} and Eu^{3+} co-doped phosphors have been used in the studies of W-LEDs, such as $Sr_2P_2O_7$:Tb^{3+}, Eu^{3+},[6] $KCaY(PO_4)_2$:Tb^{3+}, Eu^{3+},[11] $LaPO_4$:Tb^{3+}, Eu^{3+}, Bi^{3+}.[12]

For all we know, for $Ba_{1-x-y}P_2O_7$:xEu^{3+}, yTb^{3+} phosphors, its luminescence properties and the mechanism of $Tb^{3+} \rightarrow Eu^{3+}$ energy transfer have not been investigated in the previous study. In this study, the phosphors $Ba_2P_2O_7$:Tb^{3+}, Eu^{3+} were synthesized by solid-state reaction method in air. The crystal structure, photoluminescence properties, color tunability, the mechanism of $Tb^{3+} \rightarrow Eu^{3+}$ energy transfer, and luminous efficiency of prepared samples were systematically studied.

2. Experimental

2.1. Sample synthesis

The powder samples $Ba_2P_2O_7$:Tb^{3+}, Eu^{3+} were prepared by the conventional solid-state reaction in air. According to mole ratio of elements in $Ba_{1.94-y}P_2O_7$:$0.06Tb^{3+}$, yEu^{3+}, we calculated and weighed the raw materials $BaCO_3$ (A.R.), $NH_4H_2PO_4$ (A.R.), Tb_4O_7 (99.99%) and Eu_2O_3 (99.99%), and then the raw materials were fully ground in an agate mortar. Eventually, the mixtures in the alumina crucible was put into the muffle furnace and calcined at 1100 °C for 2 h. The samples were obtained after cooled to room temperature.

2.2. Sample characterization

The X-ray diffraction (XRD) patterns of the samples were recorded *via* using Japan Rigaku D/Max-2200 X-ray diffractometer with Cu-Kα radiation ($\lambda = 0.15406$ nm). The excitation and emission spectra were observed by the Hitachi F-4600

School of Materials Science and Engineering, Shaanxi University of Science and Technology, Xi'an 710021, China. E-mail: m18309293611@163.com

fluorescence spectrophotometer. Fluorescence lifetime were investigated by using the Edinburgh FS5 fluorescence spectrophotometer. All the measurements above were carried out at room temperature.

3. Results and discussion

3.1. Structure characterization

Fig. 1a and b shows the X-ray diffraction patterns of $Ba_2P_2O_7$:Tb^{3+}, Eu^{3+} and $Ba_{1.88}P_2O_7$:0.06Eu^{3+}, 0.06M^+ (Li^+, Na^+, K^+) samples, respectively. All XRD patterns are found to agree well with standard data (JCPDS 30-0144) in the $Ba_2P_2O_7$. The results indicate that the $Ba_2P_2O_7$ host keep the crystal structure when the M^+, Tb^{3+} and Eu^{3+} in small amount doping.

3.2. Luminescence properties of the $Ba_2P_2O_7$:Tb^{3+}, Eu^{3+}

Fig. 2a shows the excitation and emission spectra of $Ba_{1.94}P_2O_7$:0.06Eu^{3+} phosphor. When monitored at 593 nm, several excitation peaks at 361 nm, 381 nm and 395 nm are obtained and assigned to $^7F_0 \rightarrow {}^5D_4$, $^7F_0 \rightarrow {}^5L_7$ and $^7F_0 \rightarrow {}^5L_6$ transitions, respectively.[12,13] In the emission spectrum of $Ba_{1.94}P_2O_7$:0.06-Eu^{3+} sample, under excitation at 395 nm, the feature emission peaks are observed at 593 and 613 nm. According to the Judd–Ofelt theory,[14–16] the transition $^5D_0$–$^7F_1$ is the magnetic dipole, and it is orange emission at 593 nm. While the transition $^5D_0$–$^7F_2$ is the electric-dipole, it is red emission centered at 613 nm.

As we all know, the transition $^5D_0$–$^7F_1$ (593 nm) is the magnetic dipole, and it is insensitive to distortion of the inversion symmetry, whereas the electric dipole transition $^5D_0$–$^7F_2$ (613 nm) is hypersensitive to it, and the intensity ratio ($^5D_0$–$^7F_2$)/($^5D_0$–$^7F_1$) suggests the degree of distortion.[16] In our experiment, the transition $^5D_0$–$^7F_1$ (593 nm) was stronger than the $^5D_0$–$^7F_2$ (613 nm), this result reveals Eu^{3+} ions mainly occupy the inversion symmetry lattice site.

Fig. 2b shows the excitation and emission spectra of $Ba_{1.94}$-P_2O_7:0.06Tb^{3+}. When monitored at 545 nm, there are several excitation peaks between 300 and 380 nm, where the strongest one is at 378 nm ($^7F_6 \rightarrow {}^5D_3$).[6,10] In the emission spectrum of

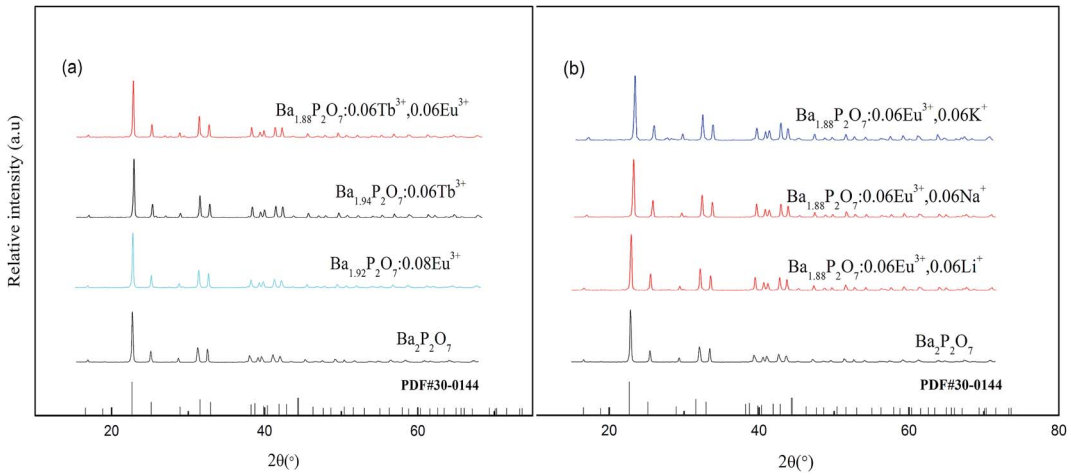

Fig. 1 XRD pattern of phosphors: (a) $Ba_{2-x-y}P_2O_7$:xTb^{3+}, yEu^{3+}, (b) $Ba_{1.88}P_2O_7$:0.06Eu^{3+}, 0.06M^+ (Li^+, Na^+, K^+).

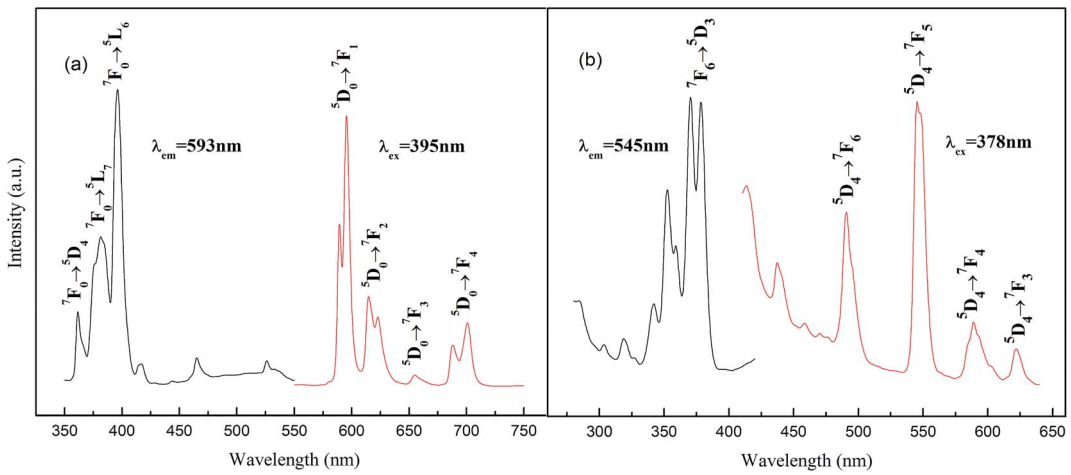

Fig. 2 Excitation and emission spectra of phosphor: (a) $Ba_{1.94}P_2O_7$:0.06Eu^{3+}, (b) $Ba_{1.94}P_2O_7$:0.06Tb^{3+}.

$Ba_{1.94}P_2O_7$:0.06Tb^{3+} sample, under excitation at 378 nm, the feature emission peaks are observed at 491, 545, 589, and 622 nm corresponding to $^5D_4$ to $^7F_6$, $^7F_5$, $^7F_4$, and $^7F_3$ transitions, respectively.[6,11]

Fig. 3 shows the emission spectra of $Ba_{1.94-y}P_2O_7$:0.06Tb^{3+}, $y$$Eu^{3+}$ samples excited at 378 nm. When doped the Eu^{3+} and Tb^{3+} in the $Ba_2P_2O_7$, the samples exhibit not only $^5D_4$ to $^7F_{6,5,4,3}$ emission bands of the Tb^{3+} ions but also the $^5D_0$–$^7F_{1,2}$ emission of the Eu^{3+} ions. When the Tb^{3+} doping concentration is 0.06, we change the doping concentration of Eu^{3+} (the concentration of 0, 0.005, 0.015, 0.02, 0.04, 0.06 and 0.08, respectively), the emission intensities of 593 and 613 nm ($^5D_0$–$^7F_{1,2}$) of Eu^{3+} are enhanced and reaches the maximum at $y = 0.06$, meanwhile the emission intensity of Tb^{3+} is impaired. This indicated that the efficient probability is notably enhanced for energy transfer (Tb^{3+} → Eu^{3+}). According to the above results, the optimal composition of Tb^{3+} and Eu^{3+} co-activated phosphor is $Ba_{1.88}P_2O_7$:0.06Tb^{3+}, 0.06Eu^{3+}, which shows the strongest emission.

From the emission intensity of sensitizer, the energy-transfer efficiency (η_{ET}) from a sensitizer to an activator can be obtained as the following equation:[8,9]

$$\eta_{ET} = 1 - \frac{I_s}{I_{s0}} \quad (1)$$

where I_{s0} is the intrinsic luminescent intensity of Tb^{3+}, I_s is the luminescent intensity of Tb^{3+} in the presence of Eu^{3+}. The energy transfer efficiencies from Tb^{3+} to Eu^{3+} excited at 378 nm are illustrated in Fig. 4. As a result, the energy transfer efficiency values from Tb^{3+} to Eu^{3+} were calculated to be 70%, 77.91%, 79.82%, 81.26%, and 79.07% for $Ba_{1.94-y}P_2O_7$:0.06Tb^{3+}, $y$$Eu^{3+}$ samples, respectively. This result reveals that the η_{ET} increases with the increase of Eu^{3+} doping content, meaning that the energy transfer from Tb^{3+} to Eu^{3+} is very efficient.

In general, for the energy transfer from a sensitizer to an activator, there are two main aspects: one is exchange interaction (the typical critical distance is no more than 5 Å) and the other is multipolar interaction (the critical distance is longer than 10 Å).[17,23,24] According to Blasse, the critical distance R_c for

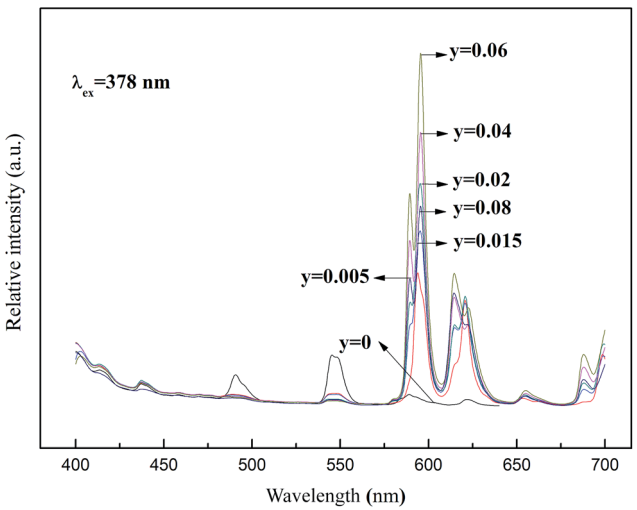

Fig. 3 The emission spectrum of $Ba_{1.94-y}P_2O_7$:0.06Tb^{3+}, $y$$Eu^{3+}$.

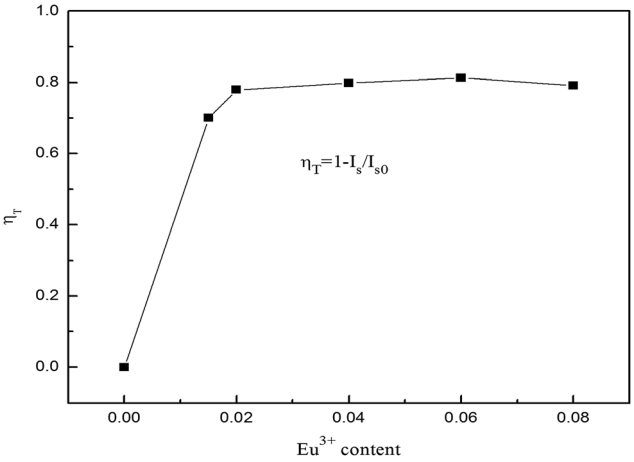

Fig. 4 Change of the energy transfer efficiency with increase of Eu^{3+} concentration.

energy transfer from the Tb^{3+} to Eu^{3+} ions can be calculated using the following equation:[18,20,26,27]

$$R_c = 2\left[\frac{3V}{4\pi x_c N}\right]^{1/3} \quad (2)$$

here, V is the unit cell volume, x_c is the critical concentration, and N is the coordinate number of molecules in the unit cell. For the $Ba_2P_2O_7$ host, $V = 543.87$ Å^3, $N = 3$, and $x_c = 0.065$ (total concentration of Tb^{3+} and Eu^{3+} when the Tb^{3+} emission intensity is half of that in the absence of Eu^{3+}). According to the above equation, the value of R_c is 17.47 Å, and it is much larger than 5 Å. So the energy transfer from Tb^{3+} to Eu^{3+} ions happen in the way of electric multipolar interaction for this system.

In order to further verify the mechanism of energy transfer for $Ba_2P_2O_7$:Tb^{3+}, Eu^{3+}, Dexter's formula of multipolar interaction and Reisfeld's approximation are used as follows:[19,21,22]

$$\frac{I_{s0}}{I_s} \propto C^{n/3} \quad (3)$$

herein, the C is the Eu^{3+} concentration, I_s is the luminescent intensity of Tb^{3+} in $Ba_2P_2O_7$:Tb^{3+}, Eu^{3+}, and I_{s0} is the intrinsic luminescent intensity of $Ba_2P_2O_7$:Tb^{3+}. Based on the eqn (3), when $n = 6$, 8, and 10 correspond to dipole–dipole, dipole–quadrupole and quadrupole–quadrupole interactions, respectively.

The I_{s0}/I_s–$C^{n/3}$ (n = 6, 8, 10) plots for $Ba_{1.94-y}P_2O_7$:0.06Tb^{3+}, $y$$Eu^{3+}$ (at excitation wavelength of 378 nm and emission wavelength of 545 nm) are shown in Fig. 5. It can be seen that when $n = 6$, the I_{s0}/I_s value follows the linear growth law much better than $n = 8$ or 10. So the dipole–dipole mechanism is the mainly way for the energy transfer between Tb^{3+} and Eu^{3+} in $Ba_2P_2O_7$.

The energy-transfer mechanism of Tb^{3+} and Eu^{3+} are shown in Fig. 6. Upon 378 nm excitation, few excited Tb^{3+} ions is excited to higher energy level through Tb^{3+}:$^7F_6$–$^5D_3$ transitions, then relaxed to lower energy levels through Tb^{3+}:$^5D_3$–$^7F_{5,4,3}$ non-radiative transitions and to its lower lying Tb^{3+}:$^5D_4$ metastable state relaxed to lower energy levels through Tb^{3+}:$^5D_4$–$^7F_{5,4,3}$ transitions.

The rest of the Tb^{3+}:$^5D_3$ level transfer their energy to the Eu^{3+}:$^5G_2$ level *i.e.* the energy transfer. A fast non-radiative decay

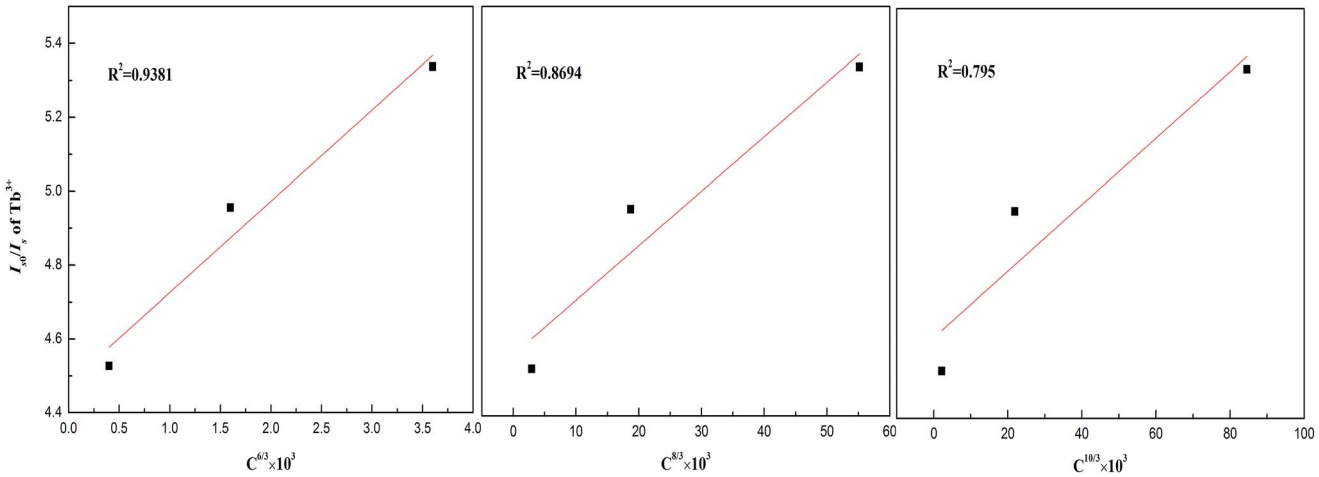

Fig. 5 Dependence of I_{s0}/I_s of Dy^{3+} on $C^{6/3}$, $C^{8/3}$ and $C^{10/3}$.

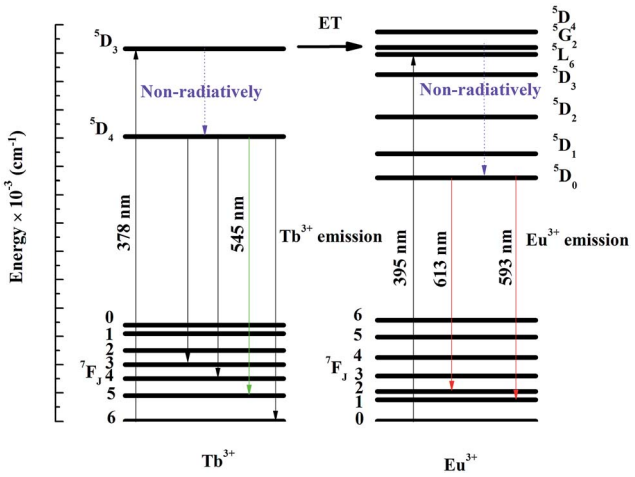

Fig. 6 Energy levels of Tb^{3+} and Eu^{3+} in $Ba_2P_2O_7$ phosphor.

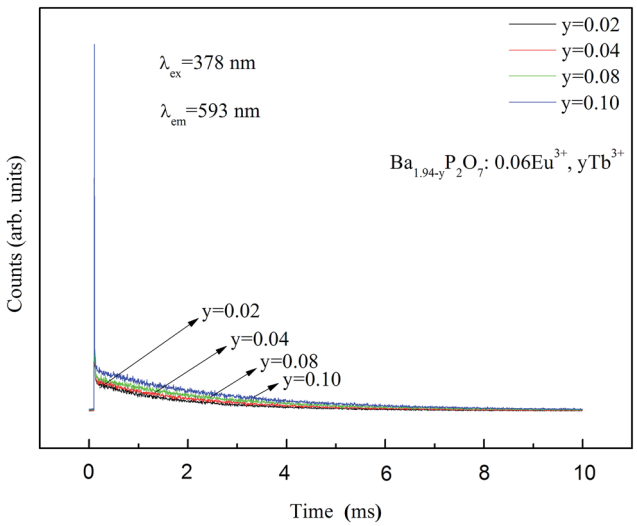

Fig. 7 PL decay curves of Eu^{3+} in $Ba_{1.94-y}P_2O_7$:$0.06Eu^{3+}$, yTb^{3+}.

from $^5G_2$ excited state increase the population of $^5D_0$ metastable state causing enhanced emission from Eu^{3+} ions through $^5D_0$–^7F_J ($J = 0$–6) transitions. Finally, the characteristic emission of Eu^{3+} at 593 and 613 nm was enhanced.

Fig. 7 shows luminescence decay for $^5D_0$ level of Eu^{3+} in $Ba_{1.94-y}P_2O_7$:$0.06Eu^{3+}$, yTb^{3+} ($y = 2\%$, 4%, 8%, 10%) excited at 378 nm and measured at 593 nm. The decay times of Eu^{3+} can be more accurate fitted *via* using second-order exponential decay mode as follows:[25]

$$I = A_1 \exp\left(-\frac{t}{\tau_1}\right) + A_2 \exp\left(-\frac{t}{\tau_2}\right) \quad (4)$$

where A_1 and A_2 are the fitting parameters, t is the time, τ_1 and τ_2 are the decay times for different exponential components, I is the phosphorescent intensity, respectively. The average decay time τ of Eu^{3+} can be expressed as the following equation:[25]

$$\tau = \frac{A_1\tau_1^2 + A_2\tau_2^2}{A_1\tau_1 + A_2\tau_2} \quad (5)$$

For $Ba_{1.94-y}P_2O_7$:$0.06Eu^{3+}$, yTb^{3+} ($y = 0.02$, 0.04, 0.08, 0.10) phosphors, corresponding to the $^5D_0$ level of Eu^{3+}, when the samples are excited at 378 nm, the average lifetimes that calculated by eqn (5) are 2.10, 2.51, 5.81, and 2.65 ms, respectively. The average decay time of Eu^{3+} increases from 2.10 to 5.81 ms as the increase of the concentration of Tb^{3+} from 0.02 to 0.08, the results confirmed the exist of energy transfer from Tb^{3+} to Eu^{3+} ions.[34,35] When the Tb^{3+} beyond 8% mol, the average decay time of Eu^{3+} is shortened oppositely, which is corresponding to the widely known concentration quenching effect happened in high concentration.

Due to Eu^{3+} and Ba^{2+} have similar radius, the Eu enter the lattice, and replace the position of the Ba^{2+} to form a point defect $Eu_{Ba}^{\cdot}$ which have a positive charge.[32,33] In order to keep the charge balance, it can be implemented by doping alkali metal ions. For $Ba_{1.94}P_2O_7$:$0.06Eu^{3+}$ phosphors, we regard Li^+ (Li_2CO_3), Na^+ (Na_2CO_3) and K^+ (K_2CO_3) as charge compensations to stabilize the structure. The results are shown in Fig. 8.

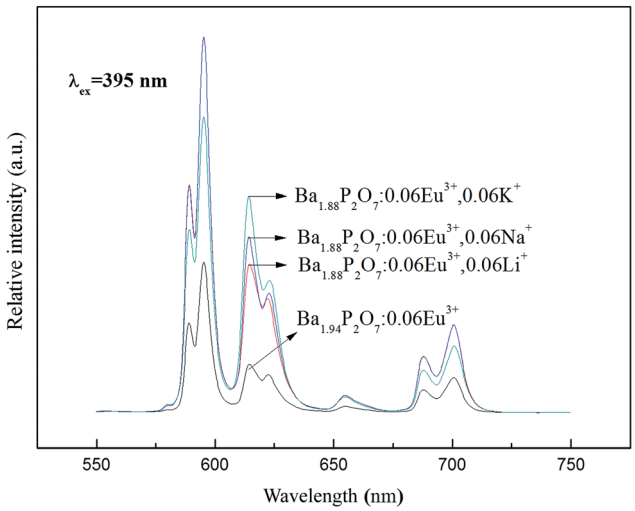

Fig. 8 Effect of Li^+, Na^+ and K^+ on the emission spectrum of $Ba_{2-x}P_2O_7$:xEu^{3+} phosphors.

When the M^+ (Li^+, Na^+, K^+) doping concentration are 0.06 respectively, the intensity of $Ba_{1.94}P_2O_7$:0.06Eu^{3+} are all enhanced. The doping Na^+ enhanced emission intensity more than by doping Li^+ or K^+ at 593 nm, and the emission intensity at 613 nm is higher by doping K^+.

Fig. 9 shows the CIE chromaticity diagram for $Ba_{2-x-y}P_2O_7$:xTb^{3+}, yEu^{3+} phosphors. According to the emission spectra, the values of CIE parameters of the $Ba_{2-x-y}P_2O_7$:xTb^{3+}, yEu^{3+} phosphors with different doping concentrations are summarized in Table 1. Under the excitation at 378 nm, the CIE coordinates of the phosphors can be tuned from blue-green (point a1, a2, a3, a4) to white (point a5), yellow (point a6, a7, a8, a9) and finally to the orange-red (point a10, a11) by changing the Eu^{3+}/Tb^{3+} ratio. The CIE chromaticity coordinates associated with white luminescence (0.358, 0.305) of $Ba_{1.94-x}P_2O_7$:0.06Tb^{3+}, 0.001Eu^{3+} sample (point a5) are very close to an ideal white chromaticity coordinates (0.33, 0.33). However, upon 395 nm excitation, the CIE chromaticity coordinates are associated with orange-red luminescence of $Ba_{2-x}P_2O_7$:xEu^{3+} phosphor (point a10, a11). Above results indicate that the phosphors show merits of multicolor emissions in the visible region when excited by a single wavelength light.

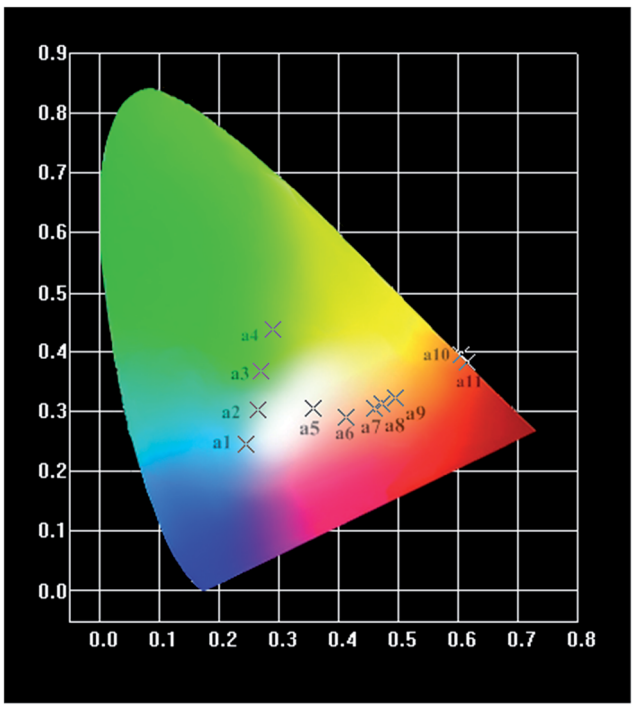

Fig. 9 CIE coordinates of the $Ba_{2-x-y}P_2O_7$:xTb^{3+}, yEu^{3+} phosphors.

Table 1 CIE chromaticity coordinates of the $Ba_{2-x-y}P_2O_7$:xTb^{3+}, yEu^{3+} phosphors

Point	Sample (λ_{ex} = 378 nm)	CIE (x, y)
a1	$Ba_{1.98}P_2O_7$:0.02Tb^{3+}	(0.245, 0.244)
a2	$Ba_{1.94}P_2O_7$:0.06Tb^{3+}	(0.264, 0.303)
a3	$Ba_{1.92}P_2O_7$:0.08Tb^{3+}	(0.271, 0.368)
a4	$Ba_{1.75}P_2O_7$:0.25Tb^{3+}	(0.291, 0.437)
a5	$Ba_{1.939}P_2O_7$:0.06Tb^{3+}, 0.001Eu^{3+}	(0.358, 0.305)
a6	$Ba_{1.935}P_2O_7$:0.06Tb^{3+}, 0.005Eu^{3+}	(0.412, 0.289)
a7	$Ba_{1.92}P_2O_7$:0.06Tb^{3+}, 0.02Eu^{3+}	(0.459, 0.304)
a8	$Ba_{1.9}P_2O_7$:0.06Tb^{3+}, 0.04Eu^{3+}	(0.473, 0.312)
a9	$Ba_{1.88}P_2O_7$:0.06Tb^{3+}, 0.06Eu^{3+}	(0.496, 0.322)
a10	$Ba_{1.985}P_2O_7$:0.015Eu^{3+} (λ_{ex} = 395 nm)	(0.604, 0.395)
a11	$Ba_{1.94}P_2O_7$:0.06Eu^{3+} (λ_{ex} = 395 nm)	(0.616, 0.383)

4. Conclusion

In summary, the $Ba_{2-x-y}P_2O_7$:xTb^{3+}, yEu^{3+} phosphors were synthesized by a solid-state reaction at 1100 °C for 2 h. The $Ba_{2-x-y}P_2O_7$:xTb^{3+}, yEu^{3+} phosphors can be effectively excited at 378 nm and have several emission peaks centered at 545 nm, 593 nm and 613 nm. The CIE coordinates of the phosphors can be tuned from blue-green to white, yellow and finally to the orange-red by changing the Eu^{3+}/Tb^{3+} ratio. The emission intensity of $Ba_{2-x}P_2O_7$:0.06Eu^{3+} was enhanced by doping charge compensation M^+ (Li^+, Na^+, K^+). The energy transfer from Tb^{3+} to Eu^{3+} in $Ba_2P_2O_7$ was demonstrated to be dipole–dipole interaction mechanism. The energy transfer efficiency in Tb^{3+}–Eu^{3+} was approximately 81.26% at x = 0.06, y = 0.06, and for the $Ba_{1.94-y}P_2O_7$:0.06Eu^{3+}, yTb^{3+} (y = 0.02, 0.04, 0.08, 0.10) phosphors, under excitation at 378 nm, the average lifetimes of Eu^{3+} were determined to be 2.10, 2.51, 5.81, and 2.65 ms, respectively.

Acknowledgements

This work was financially supported by the Innovation of Science and Technology Plan Projects of Shaanxi Province, China (Grant no. 2013KTDZ03-02-01), and by the Shaanxi University of Science and Technology Graduate Student Innovation Fund.

References

1 Z. Y. Hou, G. G. Li, H. Z. Lian and J. Lin, *J. Mater. Chem.*, 2012, **22**, 5254–5276.

2 M. M. Shang, C. X. Li and J. Lin, *Chem. Soc. Rev.*, 2014, **43**, 1372–1386.
3 S. Nizamoglu, G. Zengin and H. V. Demir, *Appl. Phys. Lett.*, 2008, **92**, 1–18.
4 C. C. Lin, Y. S. Zheng, H. Y. Chen, C. H. Ruan, G. W. Xiao and R. S. Liu, *J. Electrochem. Soc.*, 2010, **157**, 900–903.
5 H. A. Hoppe, *Angew. Chem., Int. Ed.*, 2009, **40**, 3572–3582.
6 M. Xu, L. Wang, D. Jia and H. Zhao, *J. Am. Ceram. Soc.*, 2015, **98**, 1536–1541.
7 G. G. Li, Y. Zhang, D. L. Geng, M. M. Shang, C. Peng, Z. Y. Cheng and J. Lin, *ACS Appl. Mater. Interfaces*, 2012, **4**, 296–305.
8 W. Lu, N. Guo, Y. C. Jia, Q. Zhao, W. Z. Lv, M. M. Jiao, B. Q. Shao and H. P. You, *Inorg. Chem.*, 2013, **52**, 3007–3012.
9 C. H. Huang and T. M. Chen, *J. Phys. Chem. C*, 2011, **115**, 2349–2355.
10 L. Wang, M. Xu, R. Sheng, L. Liu and D. Jia, *J. Alloys Compd.*, 2013, **579**, 343–347.
11 X. Zhang, L. Zhou, J. Shi and M. Gong, *Mater. Lett.*, 2014, **137**, 32–35.
12 Y. Xia, Y. Huang, Q. Long, S. Liao and Y. Gao, *Ceram. Int.*, 2015, **41**, 5525–5530.
13 J. A. Dorman, J. H. Choi, G. Kuzmanich and J. P. Chang, *J. Phys. Chem. C*, 2012, **116**, 12854–12860.
14 B. R. Judd, *Phys. Rev.*, 1962, **127**, 750–761.
15 G. S. Ofelt, Intensities of crystal spectra of rare-earth ions, *J. Chem. Phys.*, 1962, **37**, 511–519.
16 D. Kang, H. S. Yoo, H. J. Sang, H. Kim and D. Y. Jeon, *J. Phys. Chem. C*, 2015, **115**, 24334–24340.
17 M. Shang, D. Geng, D. Yang, X. Kang, Y. Zhang and J. Lin, *Inorg. Chem.*, 2013, **52**, 3102–3112.
18 M. Jiao, Y. Jia, W. Lü, W. Lv, Q. Zhao, B. Shao and H. You, *J. Mater. Chem. C*, 2014, **2**, 4304–4311.
19 G. Zhu, Y. Wang, Z. Ci, B. Liu, Y. Shi and S. Xin, *J. Lumin.*, 2012, **132**, 531–536.
20 G. Blasse, *Phys. Lett.*, 1968, **28**, 444–445.
21 D. L. Dexter, *J. Chem. Phys.*, 1953, **21**, 836–850.
22 R. Reisfeld, *J. Chem. Phys*, 1972, **56**, 1698–1705.
23 G. Blasse, *Philips Res. Rep.*, 1969, **24**, 131–144.
24 M. M. Shang, G. G. Li, X. J. Kang, D. M. Yang, D. L. Geng and J. Lin, *ACS Appl. Mater. Interfaces*, 2011, **3**, 2738–2746.
25 X. Qin, X. Zhang, P. He, *et al.*, *Ceram. Int.*, 2015, **41**, 5554–5560.
26 S. P. Lee, T. S. Chan and T. M. Chen, *ACS Appl. Mater. Interfaces*, 2014, **7**, 40–44.
27 S. P. Lee, C. H. Huang, T. S. Chan and T. M. Chen, *ACS Appl. Mater. Interfaces*, 2014, **6**, 7260–7267.
28 S. Pimputkar, J. S. Speck, S. P. DenBaars and S. Nakamura, *Nat. Photonics*, 2003, **3**, 180–182.
29 T. Hashimoto, F. Wu, J. S. Speck and S. Nakamura, *Nat. Mater.*, 2007, **6**, 568–571.
30 C. C. Sun, W. T. Chien, I. Moreno, C. T. Hsieh, M. C. Lin and S. L. Hsiao, *Opt. Express*, 2010, **18**, 6137–6148.
31 I. Moreno and C. C. Sun, *Opt. Express*, 2008, **16**, 1808–1819.
32 Q. Long, Y. Gao, Y. H. Huang, S. Liao and B. Song, *Mater. Lett.*, 2015, **160**, 436–439.
33 P. Li, Z. Wang, Z. Yang, Q. Guo and X. Li, *Mater. Lett.*, 2009, **63**, 751–753.
34 R. Mi, J. Chen, Y. Liu, M. Fang and L. Mei, *RSC Adv.*, 2016, **6**, 28887–28894.
35 K. Pavani, J. S. Kumar and L. R. Moorthy, *J. Alloys Compd.*, 2014, **586**, 722–729.